Defect levels in CsPbCl₃ single crystals determined by thermally stimulated current spectroscopy

John A. Peters,[1,2] Zhifu Liu,[1] Michael C. De Siena,[3] Mercouri G. Kanatzidis,[1,3] and Bruce W. Wessels[1,a]

AFFILIATIONS

[1]Department of Materials Science and Engineering, Northwestern University, Evanston, Illinois 60208, USA
[2]Department of Chemistry, Physics, and Engineering Studies, Chicago State University, Chicago, Illinois 60608, USA
[3]Department of Chemistry, Northwestern University, Evanston, Illinois 60208, USA

[a]Author to whom correspondence should be addressed: b-wessels@northwestern.edu

ABSTRACT

Thermally stimulated current (TSC) spectroscopy was used to characterize electronic trap states in the perovskite $CsPbCl_3$ bulk single crystals which are promising for gamma ray detection. The TSC spectra indicate the presence of multiple traps over the temperature range from 80 K to above room temperature. The possible analytical defects identified were V_{Cs} and V_{Cl} vacancies and Pb_i interstitials that have concentrations of the order of $10^{11}-10^{16}\,cm^{-3}$ and capture cross sections of $\sim 10^{-18}\,cm^2$. A comparison of crystals grown from different ingots reveals that the concentration of defects in the crystal with an improved growth procedure is about one to four orders of magnitude less than those of a crystal from an earlier growth process. A further reduction and elimination of trap states within the perovskite ingot should lead to crystals with improved mobilities, carrier lifetimes, and detector response characteristics.

I. INTRODUCTION

There is considerable interest in the lead halide perovskites for optoelectronic devices including light emitting diodes, photovoltaics, and hard radiation detectors. Recently, there have been marked improvements in radiation detectors fabricated from cesium lead bromide single crystals.[1–3] Nevertheless, further improvements in detector response and energy resolution are sought. Intrinsic defects are known to play a key role in controlling device performance. Even at low concentrations (at a level of parts per billion), their presence can significantly alter the properties, such as conductivity, charge-carrier mobility, minority carrier lifetime, and recombination rate, of halide semiconductors. Intrinsic defects can, therefore, deteriorate the performance of the resulting optoelectronic devices. Kang *et al.* have calculated the defect formation energies and charge transition levels of intrinsic point defects in cesium lead bromide.[4] Prior calculations in zero-dimensional perovskites indicate that most of the defects have shallow electronic transition levels and several midgap defect levels are also present but have high formation energies and low concentrations.[5] The defect concentration depends on crystal growth conditions. Previously, we showed that $CsPbCl_3$ detectors are capable of room temperature energy-resolved ⁵⁷Co and

²⁴¹Am γ-ray detection for the first time.[6] These results clearly highlight the great potential of the all-inorganic perovskite $CsPbCl_3$ for room temperature x-and γ-ray radiation detection and for this reason, we chose to begin experimental investigations aimed at better understanding the defects in this material. The question still arises, are intrinsic deep level defects present, and if so, what are their concentrations and electron trapping characteristics. Will these traps lead to unwanted noise in the detectors? Thus, detecting defects, identifying their types and densities, and then reducing/eliminating them with improved crystal growth will lead to high-quality crystals with lessened recombination loss and longer carrier lifetime which will be key issues toward improving device stability.

In this work, thermally stimulated current (TSC) measurements have been carried out over a temperature range of 80–320 K to determine the presence of deep level defects in bulk halide perovskite single crystals grown by the Bridgman technique. At low measurement temperatures, deep impurity levels in a high-resistance semiconductor can be studied by the method of TSC.[7,8] It gives quantitative information on various deep levels in a single temperature run. The energy levels and deep level defect concentrations were measured. The TSC spectra of our $CsPbCl_3$ samples were analyzed using

simultaneous peak analysis, (SIMPA),[9] which assumes that the spectrum is given by the sum of trap components where the levels act independently. Depending on the crystal growth conditions, we find that the analytical defects can vary by as much as four orders of magnitude reaching levels of 9.57×10^{16} cm^{-3}. The high levels of these defects can account for the generally high dark current observed in single crystals of this material.

II. EXPERIMENTAL AND THEORETICAL DETAILS

A. Synthesis and device fabrication

CsPbCl$_3$ was synthesized via a solid-state reaction and single crystals were grown using the Bridgman method and cleaved for optical measurements as described in our previous work.[10] Briefly, equimolar amounts of CsCl (99.999%, Sigma-Aldrich) and PbCl$_2$ (99.999%, Sigma-Aldrich) were reacted under vacuum in a sealed silica tube for 24 h at 650 °C to form CsPbCl$_3$. After synthesis, the Bridgman method was used to grow large crystals. The silica tube was heated to 620 °C for 10 h and held at that temperature for 24–48 h for overheating to avoid heterogeneous nucleation. The silica tube was then passed through a temperature gradient of 5–20 K cm^{-1} at a rate of 0.5–1 mm hr^{-1}. Once the silica tube completely passed through the temperature gradient, the ingot was cooled to room temperature at a rate of ~5 K h^{-1}. In the present study, cleaved samples taken from the tip of each ingot for TSC measurements were from two separate crystal growth processes (MCD1014 and MCD1024). The two crystals presented here were grown with different temperature gradients. Sample MCD1014 was grown with a 10–20 K cm^{-1} whereas sample MCD1024 was grown with a 5−10 K cm^{-1} gradient.

Powder x-ray diffraction (XRD) was performed on sampled cleaved perpendicularly to the length of the ingot using a Rigaku Miniflex diffractometer. Room temperature photoluminescence data were collected using an Edinburgh Instruments FS5 spectrofluorometer with a 375 nm pulsed diode laser used for excitation. Temperature dependent photoluminescence was measured using a continuous wave diode laser (OBIS 405 nm LX, 100 mW) with a constant power of 2 mW.

To conduct thermally stimulated current (TSC) spectroscopy measurements, two electrodes were used that were placed on the front and back sides of the cut wafer in a planar geometry. Electrical contacts of Bi and Au were deposited on the sample surfaces by thermal evaporation. The fabricated device was mounted on a Cu-plate placed inside a cryostat, whose temperature can be varied (between 77 and 325 K) in a controlled way by means of a PID temperature controller LabVIEW. The TSC system is able to generate ramps of temperature varying at a constant rate in the range of 2–20 K/min.

For the TSC measurements, the sample was placed in a cryostat and cooled down in the dark to 79 K with liquid nitrogen. Subsequently, at 79 K, the sample was photoexcited with a Xe arc lamp (150 W broadband wavelengths) for ~15 min to place the sample in a nonequilibrium state. About 10 min after the excitation was turned off, the sample was then heated up from 79 to 320 K with a step size of 0.5 K step. With the temperature increase in the dark from 79 to 315 K at a constant heating rate (0.10 K/s), the thermally stimulated current, the photoexcited current I_{TSC}, was obtained by a Keithley 2636 electrometer under a 15 V applied bias. Once done, the sample was cooled down again to 79 K with liquid nitrogen in the dark. Another TSC current, the dark current I_{DC}, was collected while the temperature was increased from 79 to 320 K with 0.5 K step each.

B. Theoretical considerations

TSC is an effective measurement technique used to evaluate the density of defect species. It is based on the assumption that photogenerated carriers can fill defect states at very low temperatures with temporally long enough excitation by an optical stimulus source.[11] An excitation source with energy above the bandgap generates carriers near the interface between the metal contact and crystal, whereas an excitation with below-bandgap energy has a longer penetration depth for carrier generation in the bulk. To populate trap states within both regimes, a broadband excitation source is used. The TSC technique works by first cooling down the material to a low temperature and then holding the sample at that constant temperature to allow the photogenerated carriers to relax inside of the density of states and occupy all possible trap centers. Afterward, the sample is heated slowly at a constant rate thereby thermally exciting the trapped carriers and emptying the trap centers. The released carriers can be measured as a small thermally stimulated current. A plot of current vs temperature is called the TSC spectrum. If more than one type of trap center is present, curves obtained from a TSC spectrum may be expected to show several maxima depending upon the activation energy of the centers. Carriers in shallow traps are released at low temperatures, whereas those in deep states require higher thermal energy for release and are, thus, measured at higher temperatures. Various mechanisms can give rise to a thermally stimulated current, such as emission from trap levels caused by structural defects and impurity centers, or the charge accumulation at interfaces and grain boundaries. Using a "first order kinetics" approximation under monomolecular conditions (i.e., slow re-trapping), the thermally stimulated current due to a single peak with no interference (overlaps) of other neighboring peaks is described by the following equation:

$$I = I_0 \exp\left[-\frac{E_t}{kT} - \frac{\nu}{\beta}\int_{T_0}^{T} dT e^{-\frac{E_t}{kT}} \right], \tag{1}$$

where I_0 is a pre-exponential factor, E_t is the trap activation energy (eV), k is the Boltzmann's constant (eV/K), ν is an escape frequency factor (s^{-1}), β is the heating rate (K/s), T is the absolute temperature (K), and T_0 is the temperature from which heating begins after complete filling of all deep traps. It is worth noting here that the source of the traps (i.e., bulk or surface) and their chemical nature cannot be accurately deduced from this method.

The simultaneous multiple peak analysis (SIMPA) method proposed by Pavlovic et al.[9] is utilized to resolve the spectra for a full characterization of the trap parameters, i.e., the activation energy (E_t), the capture cross section (σ_t), and the trap density (N_T). Each TSC peak (I_{TSC}), corresponding to a certain trap level in the bandgap, can be estimated by using the following equation:

$$I_{TSC} = N_T \mu \tau e A E D_t T^2$$
$$\times \exp\left\{ -\frac{E_T}{kT} - \frac{kD_t}{\beta E_T} T^4 \times e^{-E_t/kT} \times \left[1 - 4\frac{kT}{E_t} + 20\left(\frac{kT}{E_T}\right)^2 \right] \right\}, \tag{2}$$
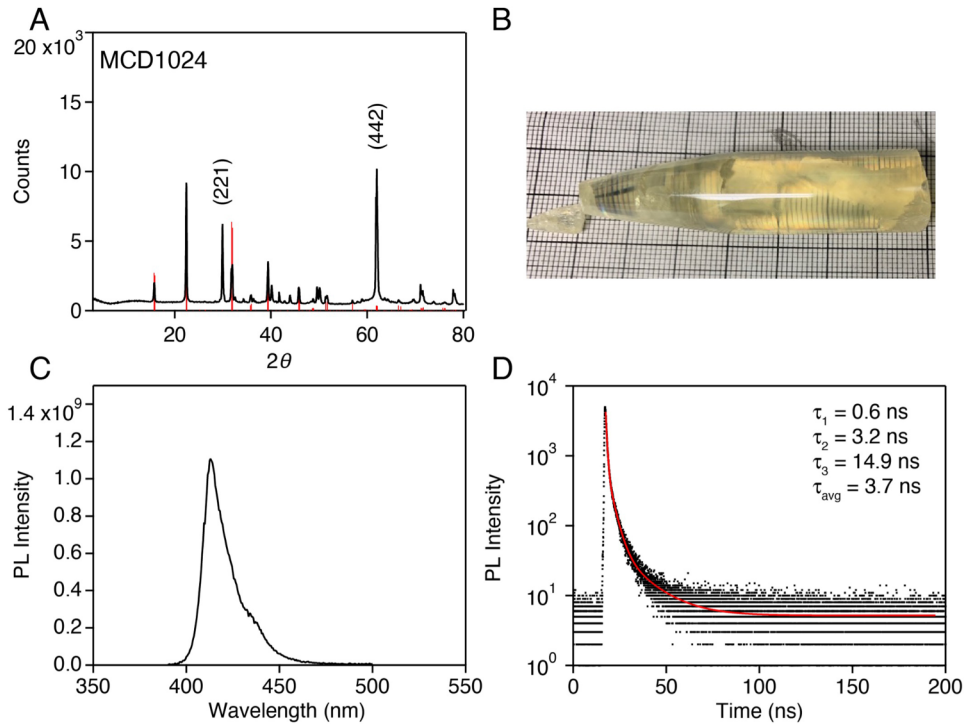
FIG. 1. (a) Powder XRD of sample MCD1024. These data index to the orthorhombic structure (*Pbnm*) of CsPbCl$_3$ and show that crystal growth occurred predominantly along the (221) direction. (b) A representative picture of a CsPbCl$_3$ ingot grown using the Bridgman crystal growth method. Steady-state (c) and time-resolved (d) photoluminescence spectra of CsPbCl$_3$ (MCD1024) taken at room temperature. The sample shows emission centered at 412 nm and multiexponential decay dynamics with an average lifetime of 3.7 ns.

where N_T is the trap density, $\mu\tau$ is the mobility-lifetime product of charge carriers, e is the electron charge, A is the electrode area, E is the applied electric field, k is the Boltzmann constant, D_t is the defect dependent coefficient, T is the absolute temperature, and E_t is the thermal activation energy of the trap level which is related to the TSC peak position. The maximum of each peak gives the approximate trap activation energy for that temperature given by

$$E_T^i = kT_m \ln\left(\frac{T_m^4}{\beta}\right). \qquad (3)$$

The temporal integration of ith individual TSC peak [Eq. (1)] yields the effective collected charge released from the ith trap
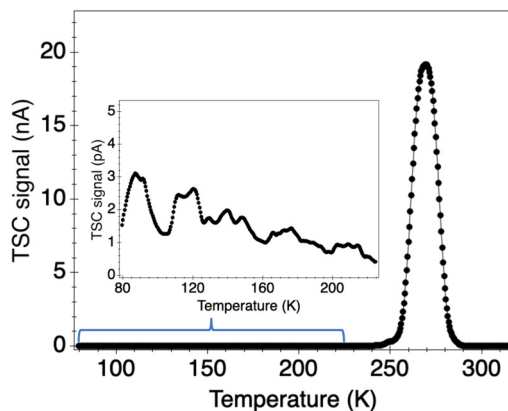

FIG. 2. The typical TSC spectrum for the solid-state CsPbCl$_3$. A series of peaks is observed over the temperature range of 80–225 K (inset).
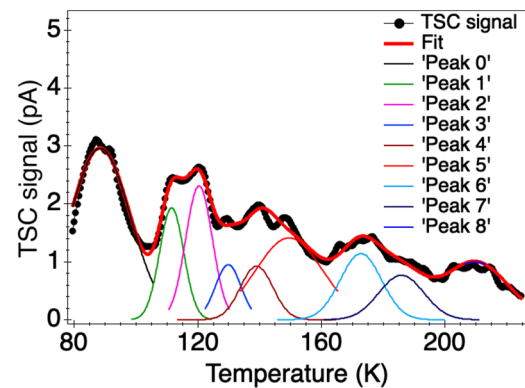

FIG. 3. TSC spectrum for a CsPbCl$_3$ single crystal (sample ID: MCD1024) prepared by the Bridgman technique. Individual peak contributions from the SIMPA fitting are presented as thin solid curves.
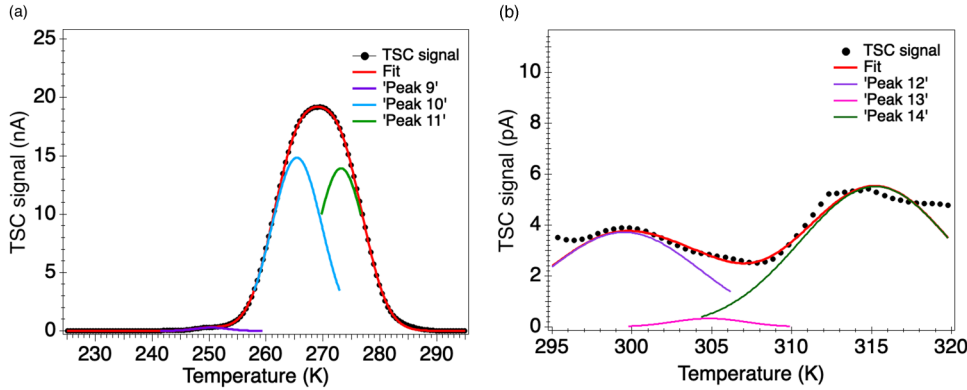
FIG. 4. (a) TSC spectrum for CsPbCl₃ (sample ID: MCD1024) from 225 to 295 K. The main peak at 270 K can be further resolved into two peaks. (b) High temperature TSC spectrum from 295 to 320 K. The peaks are three orders of smaller than the peak at 270 K.

level, i.e.,

$$Q_T^i = \int I_{TSC}^i dt = \frac{1}{\beta} \int_{T_0}^T I_{TSC}^i dT, \tag{4}$$

where $dt = \frac{dT}{\beta}$. Using Eq. (3), the ith defect concentration (N_T^i) can be expressed as

$$N_T^i = \frac{Q_T^i}{2\mu\tau eAE}. \tag{5}$$

The capture cross section σ_t for each observed trap state is calculated using the following expression:

$$\sigma_t^i = \frac{\beta E_t^2}{(E_t + 4kT_m)N\nu_{th}kT_m^2} \exp\left(\frac{E_t}{kT_m}\right). \tag{6}$$

III. RESULTS AND DISCUSSION

Knowing the distributions of trap states with respect to both location and energy is important to comprehend the influence of the traps on charge transport and recombination for device performance. Here, we probed the effect of Bridgman crystal growth conditions of CsPbCl₃ (e.g., temperature gradient and cooling profile) on defect concentration. Such different growth conditions can drastically affect the presence and quantity of macroscale extrinsic defects such as crystal cracks and twinning. Moreover, the temperature profile and cooling profiles can affect the final distribution of defects owing to changes in defect diffusion along the different gradients.

Figure 1 shows the typical characterization of the CsPbCl₃ material (sample MCD1024) studied in this work. The powder XRD in Fig. 1(a) is taken from a slice of the ingot perpendicular to the growth direction. As this is powder XRD of a single crystal sample, the data show which crystallographic plane on which growth occurs. The pattern indexes to the orthorhombic structure (*Pbnm*) of CsPbCl₃ showing growth predominantly along the (221)

TABLE I. Defect-related parameters of CsPbCl₃ (sample ID: MCD1024), obtained from the SIMPA fitting of the TSC peaks presented in Figs. 2–4. Total $N_T = 1.09 \times 10^{16}$ cm⁻³.

| Peak number (m)	T_m (K)	E_T (eV)	N_T (cm⁻³)	σ_T (×10⁻¹⁸ cm²)	Possible defects
0	88.42	0.15	2.51×10^{12}	2.43	$[V_{Cs}]^-$
1	111.54	0.20	6.56×10^{11}	3.23	$[Pb_i]^+$
2	120.40	0.22	8.64×10^{11}	3.55	$[Pb_i]^+$
3	129.84	0.24	3.44×10^{11}	3.89	$[Pb_i]^+$
4	139.03	0.26	4.22×10^{11}	4.23	$[Pb_i]^+$
5	149.54	0.29	1.33×10^{12}	4.62	$[Pb_i]^{2+}$
6	172.76	0.34	6.60×10^{11}	5.49	$[Pb_i]^{2+}$
7	185.85	0.37	4.84×10^{11}	5.99	$[Pb_i]^{2+}$
8	209.59	0.43	9.22×10^{11}	6.92	*Extrinsic*
9	250.37	0.53	7.11×10^{13}	8.56	*Extrinsic*
10	265.41	0.56	5.68×10^{15}	9.17	*Extrinsic*
11	273.19	0.58	5.14×10^{15}	9.49	*Extrinsic*
12	299.51	0.65	1.53×10^{12}	10.60	$[V_{Cl}]^-$
13	304.83	0.66	6.47×10^{10}	10.80	$[V_{Cl}]^-$
14	315.25	0.69	2.27×10^{12}	11.20	$[V_{Cl}]^-$
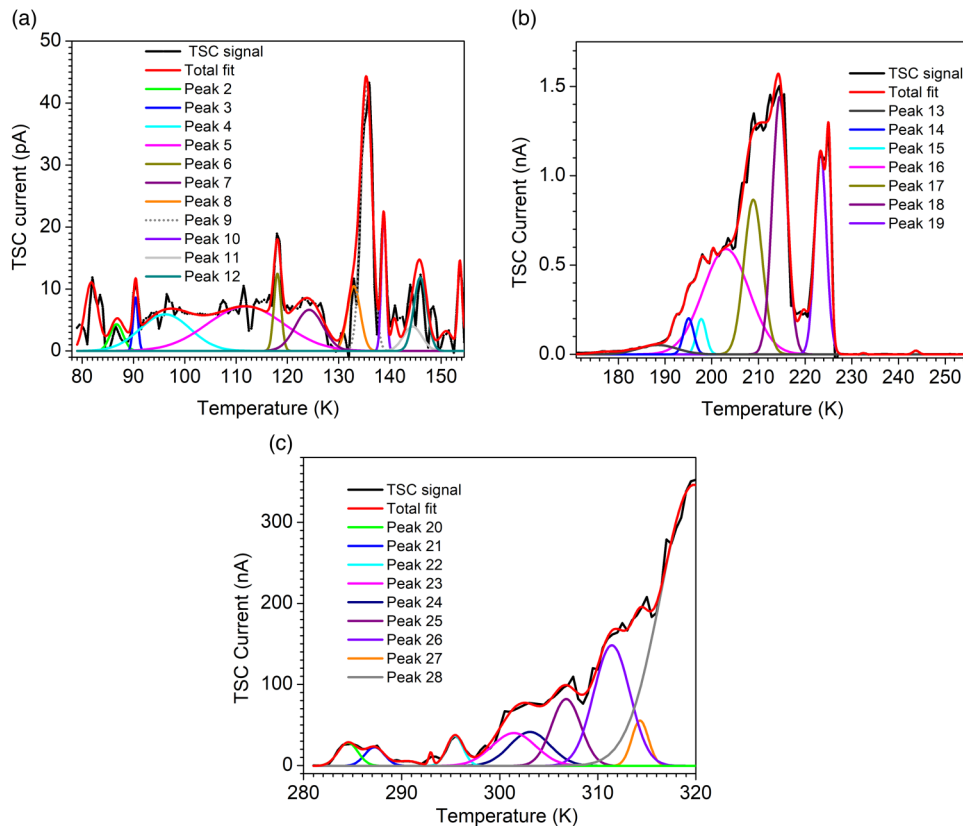
FIG. 5. TSC spectrum and SIMPA fitting for CsPbCl$_3$ (sample ID: MCD1014) from (a) 80 to 150, (b) 160 to 255, and (c) 280 to 320 K.

direction. A typical image of the as-grown ingot is given in Fig. 1(b). The ingot shows few cracks and is highly transmissive. Room temperature steady-state and time-resolved photoluminescence data are presented in Figs. 1(c) and 1(d). The sample shows strong emission centered at 412 nm with an average decay time of 3.7 ns. Sample MCD1014 shows similar luminescence behavior.

Figure 2 shows a typical TSC curve for a CsPbCl$_3$ crystal (sample ID: MCD1024) measured with a heating rate of $\beta =$ 0.1 K/s for temperature ranges 80–320 K. The TSC signal is the difference between the photoexcited current I_{TSC} and the dark current I_{DC}. The crystal was from the tip section of this ingot, i.e., the part that crystalizes first during crystal growth. A significant difference in the measured thermally stimulated current is observed, especially when the scanning temperature is higher than 240 K. The features observed in the TSC spectrum (Fig. 2, inset) indicate that there are multiple peaks of defects that always overlap each other and cannot be directly distinguished.

Figure 3 shows an experimental TSC spectrum and its SIMPA fitting results for CsPbCl$_3$ (sample ID: MCD1024) over the temperature range of 80–225 K. A series of nine peaks is observed. Figure 4 shows the TSC spectrum from 225 to 295 K [Fig. 4(a)] and from 295 to 315 K [Fig. 4(b)]. A broad peak is observed at 270 K which can be further resolved into two peaks, while three more peaks are observed between 295 and 300 K. There is very good agreement between the experimental TSC data (dotted curve)

and the SIMPA fitting routine (solid red curve) for the full temperature range ($80 \leq T \leq 320$ K).

From the best fit of the whole TSC spectra, the trap signatures, namely, E_t, N_T, and D_t can be simultaneously extracted for all traps present in the crystals, as well as the temperatures at which they are measured. In order to calculate the approximate concentration of defects in CsPbCl$_3$ crystals, the carrier mobility-lifetime product ($\mu\tau$) is required. The trap concentrations were calculated using a $\mu\tau$ value of 0.8×10^{-4} cm^2/V. The complete sets of defect parameters are calculated using Eqs. (1)–(4) and obtained simultaneously for all traps. The results are listed in Table I. The trap concentration ranges from 2×10^{11} to 5×10^{15} cm^{-3}.

As to the nature and origin of the traps observed in CsPbCl$_3$ crystals, there has been a comprehensive and in-depth research regarding the chemistry and physics of defects in the all-inorganic CsPbX$_3$.[12–14] At least four distinct groups of point defects in the CsPbX$_3$ perovskites were identified. These include vacancies (V_{Cs}, V_{Pb}, and V_X), interstitial sites (Cs_i, Pb_i, and X_i), cation substitutions (Cs_{Pb} and Pb_{Cs}), and four types of antisite substitutions (Cs_X, Pb_X, X_{Cs}, and X_{Pb}), where the antisite A_B indicates that A is substituted by B. From Table I, we observe that Trap T_o has an activation energy of 0.15 eV and a capture cross section 2.43×10^{-18} cm^2. Traps T_1—T_4 have energies in the range $0.2 \leq E_T \leq 0.26$ eV with capture cross sections 3.23–4.23 $\times 10^{-18}$ cm^2. According to the previous theoretical calculations,[4] the corresponding energies of 0.15

TABLE II. Defect-related parameters of $CsPbCl_3$ (sample ID: MCD1014), obtained from the SIMPA fitting of the TSC peaks presented in Fig. 5. Total $N_T = 2.48 \times 10^{17}$ cm^{-3}.

Peak number (m)	T_m (K)	E_T (eV)	N_T (cm^{-3})	σ_T ($\times 10^{-18}$ cm^2)	Possible defects
1–4	81.8–96.2	0.14–0.17	4.87–10.0×10^{12}	2.55–3.11	$[V_{Cs}]^-$
5–7	111.9–131.5	0.20–0.26	3.04–18.7×10^{12}	3.74–4.61	$[Pb_i]^+$
8–12	135.4–151.0	0.27–0.29	1.42–5.24×10^{12}	4.85–5.37	$[Pb_i]^+$
13–15	188.4–197.8	0.36–0.40	7.05–7.50×10^{13}	7.0–7.41	$[Pb_i]^{2+}$
16	203.5	0.42	1.02×10^{15}	7.65	*Extrinsic*
17	208.90	0.44	5.97×10^{14}	7.91	*Extrinsic*
18	214.56	0.45	8.00×10^{14}	8.17	*Extrinsic*
19	223.31	0.47	4.89×10^{14}	8.57	*Extrinsic*
20	284.50	0.62	1.01×10^{16}	1.40	*Extrinsic*
21	287.20	0.63	8.02×10^{15}	11.50	*Extrinsic*
22	295.40	0.65	1.01×10^{16}	11.90	*Extrinsic*
23	301.40	0.66	3.14×10^{16}	12.20	$[V_{Cl}]^-$
24	305.52	0.67	3.04×10^{16}	12.40	$[V_{Cl}]^-$
25	306.8	0.68	4.29×10^{16}	12.50	$[V_{Cl}]^-$
26	311.4	0.69	9.57×10^{16}	12.70	$[V_{Cl}]^-$
27	314.3	0.70	1.65×10^{16}	12.80	$[V_{Cl}]^-$

and 0.20–0.26 eV for trap T_o and traps T_1—T_4 correspond to cesium vacancy $[V_{Cs}]^-$ (acceptor, hole-types) and lead interstitial $[Pb_i]^{1+}$ (donor, electron-type) defects, respectively. Traps T_5—T_7, with energy in the range 0.29–0.37 eV, are identified as Pb interstitials $[Pb_i]^{2+}$. Traps T_8–T_{11} may be associated with other native defect complexes or other extrinsic defects such as dopants or impurities. Impurity defects are often found in the starting materials and may have been introduced during crystal growth. The total concentration of extrinsic defects (traps T_8–T_{11}) is 1.09×10^{16} cm^{-3}. Traps T_{10} and T_{11} have E_T of 0.56 and 0.58 eV, respectively, and these two traps have the highest concentration of $\sim 5 \times 10^{15}$ cm^{-3}. The concentrations for traps T_o–T_{11} range from 10^{11} to 10^{15} cm^{-3}. Recent *ab initio* calculations on slabs of $CsPbX_3$ (X = I, Br, and Cl) with a halide vacancy introduced on the surface show that halide vacancies are shallow in $CsPbI_3$, slightly deeper in $CsPbBr_3$, and close to midgap in $CsPbCl_3$.[15] Thus, traps T_{10} and T_{11} observed in Table I can be attributed to chlorine vacancies $[V_{Cl}]^-$ with a total concentration of 4.43×10^{12} cm^{-3}. $[V_{Cl}]^-$ can form by migration of Cl ions in the $CsPbCl_3$ to interstitial sites since the Pb–Cl bonds are relatively weak. Cl vacancy is believed to yield deep levels located within the middle of the bandgap.[16,17]

Figure 5 shows the experimental TSC spectrum and its SIMPA fitting results for a different $CsPbCl_3$ crystal (sample ID: MCD1014) grown from another ingot and different from that shown in Figs. 2–4. The corresponding defect-related parameters are presented in Table II. A mobility-lifetime value, $\mu\tau$, of 1.0×10^{-4} cm^2/V was used for the estimation of the TSC related parameters. This mobility-lifetime value is expected to yield an upper limit on the sum of deep level defect densities. Note that the last peak at ~ 315 K was not included in the table as its origin may be argued to be due to ionic conductivity. Moreover, the concurrent phase transition at this temperature further complicates an assignment of this peak.

A comparison of trap concentrations shown in Tables I and II reveals that the concentration of defect levels in sample MCD1024

is about one to four orders of magnitude less than that of sample MCD1014. It is worth noting that the total concentration of extrinsic defects in sample MCD1024 is of the same order (1.09×10^{16} cm^{-3}) as that of MCD1014 (2.10×10^{16} cm^{-3}). This indicates that the extrinsic defects in the two crystals are presumably of the same origin, i.e., impurities in the starting materials that may have been introduced during crystal growth, and is consistent with both samples using the same starting reagents. We also observe from Table I that the total concentration of Cl vacancies in the MCD1024 single crystal (T_{12}–T_{14}) is $\sum_{T_m=12}^{14} N_{T_m} = 3.87 \times 10^{12}$ cm^{-3} whereas the total concentration in MCD1014 (T_{23}–T_{27}) is $\sum_{T_m=23}^{27} N_{T_m} = 2.17 \times 10^{17}$ cm^{-3} (Table II). This much
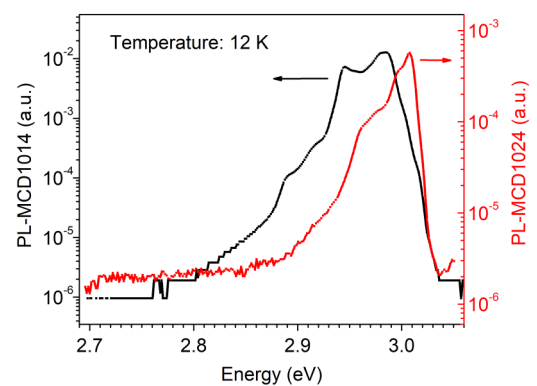
FIG. 6. Near band edge spectra for exciton emission for $CsPbCl_3$ at 12 K, over the energy range of 2.7–3.05 eV, showing band tail effects for energies less than 2.95 eV. Band tailing is dominant in sample MCD1014 (black) in comparison to sample MCD1024 (red).

lower concentration of deep levels for sample MCD1024 is in agreement with the observation from the photoluminescence (PL) response of MCD1014 and MCD1024 $CsPbCl_3$ crystals shown in Fig. 6. Both PL spectra were obtained at a temperature of 12 K with a 405 nm diode laser at a power of 2 mW. Band tailing was observed for both crystals, yet it is evident that for MCD1014, this tailing effect is more clearly seen and the PL intensity is much higher than that of the MCD1024 $CsPbCl_3$ crystal. The very broad width of PL spectra is usually an indication that the emissions are from various defects and impurity centers located near together inside the bandgap indicating a higher number of defects. Consequently, further purification of the starting materials as well as growing under a chlorine-rich environment should reduce the defect concentration and improve crystal quality and detector efficiency through vacancy reduction.

IV. CONCLUSIONS

In summary, defect levels in bulk halide perovskite $CsPbCl_3$ single crystals were examined by TSC measurements over a temperature range of 80–320 K. Three possible intrinsic point defects, namely, Cs and Cl vacancies and Pb interstitials, were found in the $CsPbCl_3$. Extrinsic defects, presumably impurities in the starting materials that may have been introduced during crystal growth, were also identified. It is found that TSC is sensitive to defect density as low as the order of $10^{11}/cm^3$, and parameters obtained through TSC can be used as feedback for crystal growth with the aim of reducing those unfavorable defect states. Among the observed defects, $[V_{Cl}]^-$ has the highest concentration of $2.17 \times 10^{17} \, cm^{-3}$. Thus, this work suggests that growing under higher chlorine vapor pressure should reduce the electron trap concentration and improve detector efficiency through vacancy reduction. A preliminary comparative study on two $CsPbCl_3$ single crystals (MCD1014 vs MCD1024) shows that the concentration of defects in the sample with an improved growth procedure (MCD1024) is about one to four orders of magnitude lower than in MCD1014. The high level of these defects can account for the generally high dark current observed in single crystals of this material.[6,18,19] The comparison of TSC spectra supports the claim that reduction/elimination of the trapping sites within the ingot should lead to crystals with improved mobilities, carrier lifetimes, and detector response characteristics.

AUTHOR DECLARATIONS
Conflict of Interest

The authors have no conflicts to disclose.

Author Contributions

John A. Peters: Formal analysis (equal); Writing – original draft (lead); Writing – review & editing (equal). **Zhifu Liu:** Formal analysis (equal); Resources (equal); Writing – review & editing (equal). **Mercouri G. Kanatzidis:** Funding acquisition (equal); Supervision (lead). **Bruce W. Wessels:** Conceptualization (lead); Funding acquisition (equal); Writing – original draft (supporting).

DATA AVAILABILITY

The data that support the findings of this study are available from the corresponding author upon reasonable request.

REFERENCES

[1]Y. He, M. Petryk, Z. Liu, D. G. Chica, I. Hadar, C. Leak, W. Ke *et al.*, "CsPbBr₃ perovskite detectors with 1.4% energy resolution for high-energy γ-rays," Nat. Photonics **15**(1), 36–42 (2021).

[2]Y. He, Z. Liu, K. M. McCall, W. Lin, D. Y. Chung, B. W. Wessels, and M. G. Kanatzidis, "Perovskite CsPbBr₃ single crystal detector for alpha-particle spectroscopy," Nuclear Instruments and Methods in Physics Research Section A: Accelerators, Spectrometers, Detectors and Associated Equipment **922**, 217–221 (2019).

[3]Y. He, L. Matei, H. J. Jung, K. M. McCall, M. Chen, C. C. Stoumpos, Z. Liu *et al.*, "High spectral resolution of gamma-rays at room temperature by perovskite CsPbBr₃ single crystals," Nat. Commun. **9**(1), 1–8 (2018).

[4]J. Kang and L.-W. Wang, "High defect tolerance in lead halide perovskite CsPbBr₃," J. Phys. Chem. Lett. **8**(2), 489–493 (2017).

[5]J. Yin, H. Yang, K. Song, A. M. El-Zohry, Y. Han, O. M. Bakr, J.-L. Brédas, and O. F. Mohammed, "Point defects and green emission in zero-dimensional perovskites," J. Phys. Chem. Lett. **9**(18), 5490–5495 (2018).

[6]Y. He, C. C. Stoumpos, I. Hadar, Z. Luo, K. M. McCall, Z. Liu, D. Y. Chung, B. W. Wessels, and M. G. Kanatzidis, "Demonstration of energy-resolved γ-ray detection at room temperature by the CsPbCl₃ perovskite semiconductor," J. Am. Chem. Soc. **143**(4), 2068–2077 (2021).

[7]A. G. Milnes, *Deep Impurities in Semiconductors* (Wiley-Interscience, 1973), p. 226.

[8]R. H. Bube, *Photoconductivity of Solids* (Wiley, New York, 1960), p. 292.

[9]M. Pavlović, M. Jakšić, H. Zorc, and Z. Medunić, "Identification of deep trap levels from thermally stimulated current spectra of semi-insulating CdZnTe detector material," J. Appl. Phys. **104**(2), 023525 (2008).

[10]J. A. Peters, Z. Liu, C. Michael, M. G. Kanatzidis, and B. W. Wessels, "Photoluminescence spectroscopy of excitonic emission in CsPbCl₃ perovskite single crystals," J. Lumin. **243**, 118661 (2022).

[11]C. Ran, J. Xu, W. Gao, C. Huang, and S. Dou, "Defects in metal triiodide perovskite materials towards high-performance solar cells: Origin, impact, characterization, and engineering," Chem. Soc. Rev. **47**(12), 4581–4610 (2018).

[12]W. Xiang and W. Tress, "Review on recent progress of all-inorganic metal halide perovskites and solar cells," Adv. Mater. **31**(44), 1902851 (2019).

[13]E. Aydin, M. De Bastiani, and S. De Wolf, "Defect and contact passivation for perovskite solar cells," Adv. Mater. **31**(25), 1900428 (2019).

[14]J. Zhang, W. Zhao, S. Olthof, and S. Liu, "Defects in CsPbX₃ perovskite: From understanding to effective manipulation for high-performance solar cells," Small Methods **5**(11), 2100725 (2021).

[15]D. P. Nenon, K. Pressler, J. Kang, B. A. Koscher, J. H. Olshansky, W. T. Osowiecki, M. A. Koc, L.-W. Wang, and A. Paul Alivisatos, "Design principles for trap-free CsPbX₃ nanocrystals: Enumerating and eliminating surface halide vacancies with softer Lewis bases," J. Am. Chem. Soc. **140**(50), 17760–17772 (2018).

[16]Z.-J. Yong, S.-Q. Guo, J.-P. Ma, J.-Y. Zhang, Z.-Y. Li, Y.-M. Chen, B.-B. Zhang *et al.*, "Doping-enhanced short-range order of perovskite nanocrystals for near-unity violet luminescence quantum yield," J. Am. Chem. Soc. **140**(31), 9942–9951 (2018).

[17]J.-K. Chen, J.-P. Ma, S.-Q. Guo, Y.-M. Chen, Q. Zhao, B.-B. Zhang, Z.-Y. Li et al., "High-efficiency violet-emitting all-inorganic perovskite nanocrystals enabled by alkaline-earth metal passivation," Chem. Mater. **31**(11), 3974–3983 (2019).

[18]X. Zhan, X. Zhang, Z. Liu, C. Chen, L. Kong, S. Jiang, S. Xi, G. Liao, and X. Liu, "Boosting the performance of self-powered $CsPbCl_3$-based UV photodetectors by a sequential vapor-deposition strategy and heterojunction engineering," ACS Appl. Mater. Interfaces **13**(38), 45744–45757 (2021).

[19]P. Zhang, Y. Hua, Y. Xu, Q. Sun, X. Li, F. Cui, L. Liu, Y. Bi, G. Zhang, and X. Tao, "Ultrasensitive and robust 120 keV hard x-ray imaging detector based on mixed-halide perovskite $CsPbBr_{3-n}I_n$ single crystals," Adv. Mater. **34**, 2106562 (2022).